Supplementary Information for

Nonlinear Hall Effect in Insulators

He *et al.*

SUPPLEMENTARY NOTE 1: DENSITY MATRIX FORMALISM FOR THE NONLINEAR RESPONSE

In the presence of external electric and magnetic fields, the Hamiltonian of electrons in a lattice system can take the general form

$$\hat{H}(\boldsymbol{r},t) = -\frac{\hbar^2}{2m}\left[\nabla + i\frac{e}{\hbar}\boldsymbol{A}(\boldsymbol{r},t)\right]^2 + V(\boldsymbol{r}) - eA_0(\boldsymbol{r},t), \tag{1}$$

with $V(\boldsymbol{r})$ being the periodic lattice potential, $A_0(\boldsymbol{r},t)$ and $\boldsymbol{A}(\boldsymbol{r},t)$ denoting the electromagnetic $U(1)$ gauge fields. Here the electric field takes the form $\boldsymbol{E}(\boldsymbol{r},t) = -\partial_t \boldsymbol{A}(\boldsymbol{r},t) - \nabla A_0(\boldsymbol{r},t)$, and the magnetic field reads $\boldsymbol{B}(\boldsymbol{r},t) = \nabla \times \boldsymbol{A}(\boldsymbol{r},t)$. There are two types of gauge choices to consider the perturbation effects induced by the electromagnetic fields. One is the length gauge and the other is the velocity gauge. The two have been proved to be equivalent through a gauge transformation [1]. In this work, we mainly consider the effect of an uniform external electric field, so we choose to take the length gauge $\boldsymbol{E}(t) = -\nabla A_0(\boldsymbol{r},t)$ to proceed. In the length gauge description, the Hamiltonian in Eq. 1 becomes

$$\hat{H}(\boldsymbol{r},t) = \hat{H}_0(\boldsymbol{r}) + e\boldsymbol{E}(t)\cdot\boldsymbol{r}, \qquad \text{with} \qquad \hat{H}_0(\boldsymbol{r}) = -\frac{\hbar^2}{2m}\nabla^2 + V(\boldsymbol{r}). \tag{2}$$

Since $\hat{H}_0(\boldsymbol{r})$ respects the translation symmetry, the eigenstate of $\hat{H}_0(\boldsymbol{r})$ is known to be the the Bloch state. In the Dirac notation, the eigen equation of the Bloch state reads

$$\hat{H}_0|\psi_{n,\boldsymbol{k}}\rangle = E_{n,\boldsymbol{k}}|\psi_{n,\boldsymbol{k}}\rangle, \quad \text{with} \quad |\psi_{n,\boldsymbol{k}}\rangle = e^{i\boldsymbol{k}\cdot\boldsymbol{r}}|u_{n,\boldsymbol{k}}\rangle. \tag{3}$$

Here $E_{n,\boldsymbol{k}}$ is the energy dispersion of the band n, and $|u_{n,\boldsymbol{k}}\rangle$ denotes periodic part of the Bloch function. The corresponding density matrix operator reads

$$\hat{\rho}_0 = \frac{1}{1+e^{(\hat{H}_0-\mu)/k_bT}} = \sum_n \frac{|\psi_{n,\boldsymbol{k}}\rangle\langle\psi_{n,\boldsymbol{k}}|}{1+e^{(E_{n,\boldsymbol{k}}-\mu)/k_bT}}. \tag{4}$$

In an external electric field $\boldsymbol{E}(t) = \boldsymbol{\mathcal{E}}(\omega)e^{-i\omega t} + \boldsymbol{\mathcal{E}}(-\omega)e^{i\omega t}$, the coupling between the electrons in the lattice and the external electric field gives rise to a series of nonlinear order electric current. In the second order, the electric current density takes the form

$$J_q(t) = J_q(2\omega)e^{-i2\omega t} + J_q(-2\omega)e^{i2\omega t} + J_q(0), \tag{5}$$

with

$$J_q(2\omega) = \sigma_{qij}(2\omega;\omega,\omega)\mathcal{E}_i(\omega)\mathcal{E}_j(\omega), \quad \text{and} \quad J_q(0) = \sigma_{qij}(0;\omega,-\omega)\mathcal{E}_i(\omega)\mathcal{E}_j(-\omega) + \sigma_{qij}(0;-\omega,\omega)\mathcal{E}_i(-\omega)\mathcal{E}_j(\omega) \tag{6}$$

denoting the second harmonic generation and rectification respectively. Here the repeated indices imply to do the summation. As the external electric field induces nonequilibrium distribution of the Bloch states, the Bloch electrons start to move away from their original positions, giving rise to electric current in response to the external electric field. One standard method to deal with the nonliear response of Bloch electrons to external electric fields is the density matrix formalism [1–4]. Applying the density matrix formalism, we obtain the conductivity of the second harmonic current

$$\sigma_{qij}(2\omega;\omega,\omega) = \frac{e^3}{2\hbar}\int_{\boldsymbol{k}}\sum_a f_{a,\boldsymbol{k}}\left\{\left[\hat{D}^i, \frac{1}{\hbar\bar{\omega}+\Delta E}\circ\left[\hat{D}^j, \frac{1}{2\hbar\bar{\omega}+\Delta E}\circ\left[\hat{D}^q,\hat{H}_0\right]\right]\right]_{aa,\boldsymbol{k}} + (i\leftrightarrow j)\right\} \tag{7}$$

and the conductivity of the rectification current

$$\begin{aligned}\sigma_{qij}(0;\omega,-\omega) = \frac{e^3}{2\hbar}\int_{\boldsymbol{k}}\sum_a f_{a,\boldsymbol{k}}\Bigg\{&\left[\hat{D}^i, \frac{1}{\hbar\bar{\omega}+\Delta E}\circ\left[\hat{D}^j, \frac{1}{i2\hbar\tau^{-1}+\Delta E}\circ\left[\hat{D}^q,\hat{H}_0\right]\right]\right]_{aa,\boldsymbol{k}} \\ &+\left[\hat{D}^j, \frac{1}{-\hbar\bar{\omega}^*+\Delta E}\circ\left[\hat{D}^i, \frac{1}{i2\hbar\tau^{-1}+\Delta E}\circ\left[\hat{D}^q,\hat{H}_0\right]\right]\right]_{aa,\boldsymbol{k}}\Bigg\}.\end{aligned} \tag{8}$$

Here $f_{a,\boldsymbol{k}} = \langle\psi_{a,\boldsymbol{k}}|\hat{\rho}_0|\psi_{a,\boldsymbol{k}}\rangle = \frac{1}{1+e^{(E_{a,\boldsymbol{k}}-\mu)/k_bT}}$ denotes the Fermi Dirac distribution of the Bloch state $|\psi_{a,\boldsymbol{k}}\rangle$, $\left(\hat{A}\circ\hat{B}\right)_{ab} = \hat{A}_{ab}\hat{B}_{ab}$ is the Hadamard product, and $\left[\hat{A},\hat{B}\right]_{ab} = \sum_c\left(\hat{A}_{ac}\hat{B}_{cb} - \hat{B}_{ac}\hat{A}_{cb}\right)$ means the commutator. Please note that

we have defined the complex frequency: $\bar{\omega} = \omega + i\tau^{-1}$ with τ being a phenomenological parameter that denotes the relaxation time. In the derivation of Eq. 7 and Eq. 8, we have assumed that the external electric field is adiabatically switched on [1]. Eq. 7 and Eq. 8 indicate that the second order conductivities are given by the trace of a series of nested commutator. In the calculation, all the operators in the commutators are expressed as matrices in the Bloch basis; for example, $\Delta E_{ab,\boldsymbol{k}} = E_{a,\boldsymbol{k}} - E_{b,\boldsymbol{k}}$. Specifically, $\hat{\boldsymbol{D}}$ in the commutator is the covariant derivative operator [1, 4]. In the Bloch basis, the matrix elements for a commutator that involves $\hat{\boldsymbol{D}}$ are

$$\left[\hat{\boldsymbol{D}}, \hat{S}\right]_{ab,\boldsymbol{k}} = \left[\hat{\boldsymbol{D}}, \hat{S}\right]^{(1)}_{ab,\boldsymbol{k}} + \left[\hat{\boldsymbol{D}}, \hat{S}\right]^{(2)}_{ab,\boldsymbol{k}}, \tag{9}$$

with

$$\left[\hat{\boldsymbol{D}}, \hat{S}\right]^{(1)}_{ab,\boldsymbol{k}} = \partial_{\boldsymbol{k}} \hat{S}_{ab,\boldsymbol{k}} - i\Delta \boldsymbol{A}_{ab,\boldsymbol{k}} \hat{S}_{ab,\boldsymbol{k}}, \qquad \left[\hat{\boldsymbol{D}}, \hat{S}\right]^{(2)}_{ab,\boldsymbol{k}} = -i\left(\sum_{c\neq a} \boldsymbol{A}_{ac,\boldsymbol{k}} \hat{S}_{cb,\boldsymbol{k}} - \sum_{c\neq b} \hat{S}_{ac,\boldsymbol{k}} \boldsymbol{A}_{cb,\boldsymbol{k}}\right). \tag{10}$$

Here $\hat{S}_{ab,\boldsymbol{k}} = \langle \psi_{a,\boldsymbol{k}} | \hat{S} | \psi_{b,\boldsymbol{k}} \rangle$ means an operator in the Bloch basis, $\boldsymbol{A}_{ab,\boldsymbol{k}} = i \langle u_{a,\boldsymbol{k}} | \partial_{\boldsymbol{k}} u_{b,\boldsymbol{k}} \rangle$ is the non-Abelian Berry connection, and $\Delta \boldsymbol{A}_{ab,\boldsymbol{k}} = \boldsymbol{A}_{aa,\boldsymbol{k}} - \boldsymbol{A}_{bb,\boldsymbol{k}}$. When $a = b$, the non-Abelian Berry connection reduces to the Abelian Berry connection: $\boldsymbol{A}_{a,\boldsymbol{k}} = i \langle u_{a,\boldsymbol{k}} | \partial_{\boldsymbol{k}} u_{a,\boldsymbol{k}} \rangle$. It is important to note that the commutators in Eq. 9 and Eq. 10 all respect the gauge invariance. With Eq. 9 and Eq. 10, we are ready to proceed with the calculation of the second order conductivities in Eq. 7 and Eq. 8.

SUPPLEMENTARY NOTE 2: THE LONGITUDINAL AND TRANSVERSE COMPONENTS OF THE NONLINEAR RESPONSE

For the nonlinear current response $J_q(\omega) = \sigma_{qij}(\omega; \omega_1, \omega_2) \mathcal{E}_i(\omega_1) \mathcal{E}_j(\omega_2)$, it is known that one can simultaneously interchange the two fields $\mathcal{E}_i(\omega_1)$, $\mathcal{E}_j(\omega_2)$, and such interchange does not affect the result. This is the intrinsic permutation symmetry of the nonlinear conductivity [5, 6]. It can be seen from Eq. 7 and Eq. 8 that both $\sigma_{qij}(2\omega; \omega, \omega)$ and $\sigma_{qij}(0; \omega, -\omega)$ respect the intrinic permutation symmetry:

$$\sigma_{qij}(2\omega; \omega, \omega) = \sigma_{qji}(2\omega; \omega, \omega), \qquad \sigma_{qij}(0; \omega, -\omega) = \sigma_{qji}(0; -\omega, \omega). \tag{11}$$

However, the output index q is not subjected to any permutation symmetry. By interchanging the output index q with the input indices i and j, one can get both the symmetric and anti-symmetric part of the nonlinear conductivity. The symmetric part, which we refer to the longitudinal component, is the ordinary Ohm like conductivity, while the anti-symmetric part, which we refer to the transverse component, is the nonlinear Hall conductivity.

The Longitudinal and Transverse Decomposition of the Second Harmonic Generation

Constructing the longitudinal and transverse components of the nonlinear conductivity basically follows 2 rules: 1) interchanging q with i and j gives a positive sign for the longitudinal component and a negative sign for the transverse component in the corresponding interchange channel; 2) the resulting longitudinal and transverse conductivity respects the intrinsic permutation symmetry. For the conductivity of second harmonic generation, we then found that its longitudinal and transverse components are constructed as

$$\sigma^{\parallel}_{qij}(2\omega; \omega, \omega) = \frac{1}{3}\left[\sigma_{qij}(2\omega; \omega, \omega) + \sigma_{iqj}(2\omega; \omega, \omega) + \sigma_{jiq}(2\omega; \omega, \omega)\right], \tag{12}$$

$$\begin{aligned}\sigma^{\perp}_{qij}(2\omega; \omega, \omega) =& \frac{1}{3}\left[\sigma_{qij}(2\omega; \omega, \omega) - \sigma_{iqj}(2\omega; \omega, \omega) + \sigma_{qij}(2\omega; \omega, \omega) - \sigma_{jiq}(2\omega; \omega, \omega)\right] \\ =& \frac{1}{3}\left[2\sigma_{qij}(2\omega; \omega, \omega) - \sigma_{iqj}(2\omega; \omega, \omega) - \sigma_{jiq}(2\omega; \omega, \omega)\right].\end{aligned} \tag{13}$$

It is evident that the summation of longitudinal component $\sigma^{\parallel}_{qij}(2\omega; \omega, \omega)$ and the transverse component $\sigma^{\perp}_{qij}(2\omega; \omega, \omega)$ recovers the second harmonic conductivity: $\sigma_{qij}(2\omega; \omega, \omega) = \sigma^{\parallel}_{qij}(2\omega; \omega, \omega) + \sigma^{\perp}_{qij}(2\omega; \omega, \omega)$. Both $\sigma^{\parallel}_{qij}(2\omega; \omega, \omega)$ and $\sigma^{\perp}_{qij}(2\omega; \omega, \omega)$ respect the intrinsic permutation symmetry. For the longitudinal component $\sigma^{\parallel}_{qij}(2\omega; \omega, \omega)$, it respects

the overall permutation symmetry for all the indices q, i, j. For the transverse component $\sigma^{\perp}_{qij}(2\omega;\omega,\omega)$, its form can be further simplified to be

$$\begin{aligned}\sigma^{\perp}_{qij}(2\omega;\omega,\omega) =& \frac{1}{3}\left[\epsilon_{lqj}\epsilon_{lab}\sigma_{aib}(2\omega;\omega,\omega) + (i \leftrightarrow j)\right] \\ =& \epsilon_{ljq}\gamma_{il}(\omega) + (i \leftrightarrow j),\end{aligned} \tag{14}$$

where $\gamma_{il}(\omega) = -\frac{1}{3}\epsilon_{lab}\sigma_{aib}(2\omega;\omega,\omega)$ is a rank-2 pseudotensor. Here ϵ_{ljq} is the Levi-Civita symbol, and the repeated indices mean to do the summation. The anti-symmetric property of $\sigma^{\perp}_{qij}(2\omega;\omega,\omega)$ when interchanging q with i and j is seen to arise from the anti-symmetric Levi-Civita symnbol. As a result, $\sigma^{\perp}_{qij}(2\omega;\omega,\omega)$ constructed in Eq. 13 and Eq. 14 corresponds to the Hall conductivity of the second harmonic generation.

The Longitudinal and Transverse Decomposition of the Rectification

One can decompose the rectification conductivity $\sigma_{qij}(0;\omega,-\omega)$ in the similar way to obtain its longitudinal and transverse components. However, since the permutation symmetry of i, j in $\sigma_{qij}(0;\omega,-\omega)$ is associated with the frequency index, the decomposition becomes a bit more complicated. For the rectification conductivity $\sigma_{qij}(0;\omega,-\omega)$, the intrinsic permutation symmetry and the reality condition implies [5, 6]

$$\sigma_{qij}(0;\omega,-\omega) = \sigma_{qji}(0;-\omega,\omega) = \left[\sigma_{qji}(0;\omega,-\omega)\right]^*, \tag{15}$$

so $\sigma_{qij}(0;\omega,-\omega)$ is Hermitian in the latter two indices. As a result, one can first decompose $\sigma_{qij}(0;\omega,-\omega)$ as

$$\sigma_{qij}(0;\omega,-\omega) = \eta_{qij}(\omega) + i\kappa_{qij}(\omega) \tag{16}$$

with

$$\eta_{qij}(\omega) = \frac{1}{2}\left[\sigma_{qij}(0;\omega,-\omega) + \sigma_{qji}(0;\omega,-\omega)\right], \qquad \kappa_{qij}(\omega) = -\frac{i}{2}\left[\sigma_{qij}(0;\omega,-\omega) - \sigma_{qji}(0;\omega,-\omega)\right]. \tag{17}$$

Here $\eta_{qij}(\omega) = \eta_{qji}(\omega)$ denotes the linear photo-galvanic effect, while $\kappa_{qij}(\omega) = -\kappa_{qji}(\omega)$ denotes the circular photo-galvanic effect [7]. The longitudinal and transverse decomposition of $\eta_{qij}(\omega)$ follows exactly as what has been done in the second harmonic generation:

$$\eta^{\parallel}_{qij}(\omega) = \frac{1}{3}\left[\eta_{qij}(\omega) + \eta_{iqj}(\omega) + \eta_{jiq}(\omega)\right], \qquad \eta^{\perp}_{qij}(\omega) = \frac{1}{3}\left[2\eta_{qij}(\omega) - \eta_{iqj}(\omega) - \eta_{jiq}(\omega)\right]. \tag{18}$$

For the circular photo-galvanic conductivity $\kappa_{qij}(\omega)$ that is anti-symmetric in i and j, we know that it can be further simplified as

$$\kappa_{qij}(\omega) = -\frac{i}{2}\epsilon_{lij}\epsilon_{lab}\sigma_{qab}(0;\omega,-\omega) = -\frac{i}{2}\epsilon_{lij}\nu_{lq}(\omega), \quad \text{with} \quad \nu_{lq}(\omega) = \epsilon_{lab}\sigma_{qab}(0,\omega,-\omega). \tag{19}$$

Here $\nu_{lq}(\omega)$ is a rank-2 pseudotensor that can be decomposed into symmetric part $\nu^{+}_{lq}(\omega) = \frac{1}{2}\left[\nu_{lq}(\omega) + \nu_{ql}(\omega)\right]$ and anti-symmetric part $\nu^{-}_{lq}(\omega) = \frac{1}{2}\left[\nu_{lq}(\omega) - \nu_{ql}(\omega)\right] = \epsilon_{lqm}p_m(\omega)$ with $p_m(\omega) = \frac{1}{2}\epsilon_{mlq}\nu_{lq}(\omega)$. It is important to note that $\nu^{+}_{lq}(\omega)$ can always be diagonalized through an orthgonal transformation. Let us choose the coordinate that makes $\nu^{+}_{lq}(\omega)$ diagonalized as $\nu^{+}_{lq}(\omega) = \alpha_l(\omega)\circ\delta_{lq}$, and then transverse component of $\kappa_{qij}(\omega)$ is found to take the form:

$$\kappa^{\perp}_{qij}(\omega) = = -\frac{i}{2}\epsilon_{lij}\nu^{+}_{lq}(\omega) = -\frac{i}{2}\epsilon_{qij}\circ\alpha_q(\omega). \tag{20}$$

Substituting $\nu^{-}_{lq}(\omega) = \epsilon_{lqm}p_m(\omega)$ into Eq. 19, we find it gives the longitudinal componenent of $\kappa_{qij}(\omega)$:

$$\kappa^{\parallel}_{qij}(\omega) = -\frac{i}{2}\epsilon_{lij}\nu^{-}_{lq}(\omega) = -\frac{i}{2}\epsilon_{lij}\epsilon_{lqm}p_m(\omega) = -\frac{i}{2}\left[\delta_{iq}p_j(\omega) - \delta_{jq}p_i(\omega)\right]. \tag{21}$$

It is clear that $\kappa^{\perp}_{qij}(\omega)$ in Eq. 20 is anti-symmetric in all the three indices, while $\kappa^{\parallel}_{qij}(\omega)$ in Eq. 21 is symmetric when interchanging q with i and j. As a result, Eq. 20 and Eq. 21 indeed correspond to the longitudinal and transverse components of $\kappa_{qij}(\omega)$ in Eq. 19. With Eq. 18, Eq. 20 and Eq. 21, we are able to decompose the rectification conductivity $\sigma_{qij}(0;\omega,-\omega)$ into longitudinal and transverse components:

$$\sigma^{\parallel}_{qij}(0;\omega,-\omega) = \eta^{\parallel}_{qij}(\omega) + i\kappa^{\parallel}_{qij}(\omega), \qquad \sigma^{\perp}_{qij}(0;\omega,-\omega) = \eta^{\perp}_{qij}(\omega) + i\kappa^{\perp}_{qij}(\omega). \tag{22}$$

In recent experimental studies [8–22], since the nonlinear Hall effect is mainly identified through the second harmonic generation that is perpendicular to the applied electric field, we will focus on the Hall conductivity $\sigma^{\perp}_{qij}(2\omega;\omega,\omega)$ of the second harmonic generation in this work.

SUPPLEMENTARY NOTE 3: THE HALL CONDUCTIVITY OF THE SECOND HARMONIC GENERATION

Combining Eq. 7, Eq. 9, Eq. 10, Eq. 13 and Eq. 14, we calculate the Hall conductivity of the second harmonic generation and find that in the presence of time reversal symmetry, its explicit expression is composed of 4 terms

$$\sigma^{\perp}_{qij}\left(2\omega;\omega,\omega\right)=\epsilon_{ljq}\left[\gamma^{(1)}_{il}\left(\omega\right)+\gamma^{(2)}_{il}\left(\omega\right)+\gamma^{(3)}_{il}\left(\omega\right)+\gamma^{(4)}_{il}\left(\omega\right)\right]+\left(i\leftrightarrow j\right). \tag{23}$$

The 4 terms are integrations of products between frequency dependent quantum geometric quantities and frequency dependent form factors. The first term takes the form

$$\gamma^{(1)}_{il}\left(\omega\right)=\int_{\boldsymbol{k}}\sum_{a}\partial_{k_i}f_{a,\boldsymbol{k}}\sum_{c\neq a}\left(i\boldsymbol{A}_{ac,\boldsymbol{k}}\times\boldsymbol{A}_{ca,\boldsymbol{k}}\right)_l g^{(1)}_{ac,\boldsymbol{k}}\left(\omega\right), \tag{24}$$

with

$$g^{(1)}_{ac,\boldsymbol{k}}\left(\omega\right)=\frac{e^3}{2\hbar}\left[\frac{\tau}{\hbar\left(1-i\omega\tau\right)}+\frac{i\hbar\bar{\omega}}{\hbar^2\bar{\omega}^2-\left(\Delta E_{ac,\boldsymbol{k}}\right)^2}-\frac{4i\bar{\omega}}{4\hbar^2\bar{\omega}^2-\left(\Delta E_{ac,\boldsymbol{k}}\right)^2}\right]. \tag{25}$$

The second term has the form

$$\gamma^{(2)}_{il}\left(\omega\right)=\int_{\boldsymbol{k}}\sum_{a,c\neq a}f_{a,\boldsymbol{k}}i\left[A^{i}_{ac,\boldsymbol{k}}\left(\hat{\partial}_{\boldsymbol{k}}\times\boldsymbol{A}_{ca,\boldsymbol{k}}\right)_l-\left(\hat{\partial}_{\boldsymbol{k}}\times\boldsymbol{A}_{ac,\boldsymbol{k}}\right)_l A^{i}_{ca,\boldsymbol{k}}+\partial_{k_i}\left(\boldsymbol{A}_{ac,\boldsymbol{k}}\times\boldsymbol{A}_{ca,\boldsymbol{k}}\right)_l\right]g^{(2)}_{ac,\boldsymbol{k}}\left(\omega\right), \tag{26}$$

with

$$g^{(2)}_{ac,\boldsymbol{k}}\left(\omega\right)=\frac{i2e^3\hbar^2\bar{\omega}^3}{\left[\hbar^2\bar{\omega}^2-\left(\Delta E_{ac,\boldsymbol{k}}\right)^2\right]\left[4\hbar^2\bar{\omega}^2-\left(\Delta E_{ac,\boldsymbol{k}}\right)^2\right]}. \tag{27}$$

The third term is

$$\gamma^{(3)}_{il}\left(\omega\right)=\int_{\boldsymbol{k}}\sum_{a,c\neq a}f_{a,\boldsymbol{k}}\left[i\left(\boldsymbol{A}_{ac,\boldsymbol{k}}\times\boldsymbol{A}_{ca,\boldsymbol{k}}\right)_l\Delta E_{ac,\boldsymbol{k}}\partial_{k_i}\Delta E_{ac,\boldsymbol{k}}\right]g^{(3)}_{ac,\boldsymbol{k}}\left(\omega\right), \tag{28}$$

with

$$g^{(3)}_{ac,\boldsymbol{k}}\left(\omega\right)=\frac{i3e^3\hbar^2\bar{\omega}^3\left[8\hbar^2\bar{\omega}^2-5\left(\Delta E_{ac,\boldsymbol{k}}\right)^2\right]}{\left[4\hbar^2\bar{\omega}^2-\left(\Delta E_{ac,\boldsymbol{k}}\right)^2\right]^2\left[\hbar^2\bar{\omega}^2-\left(\Delta E_{ac,\boldsymbol{k}}\right)^2\right]^2}. \tag{29}$$

The fourth term reads

$$\gamma^{(4)}_{il}\left(\omega\right)=\int_{\boldsymbol{k}}\sum_{a,c\neq a,c_1\neq c,c_1\neq a}\left[A^{i}_{cc_1,\boldsymbol{k}}\left(i\boldsymbol{A}_{ac,\boldsymbol{k}}\times\boldsymbol{A}_{c_1a,\boldsymbol{k}}\right)_l-A^{i}_{c_1c,\boldsymbol{k}}\left(i\boldsymbol{A}_{ac_1,\boldsymbol{k}}\times\boldsymbol{A}_{ca,\boldsymbol{k}}\right)_l\right]\left[f_{a,\boldsymbol{k}}g^{(4)}_{acc_1,\boldsymbol{k}}\left(\omega\right)-f_{c,\boldsymbol{k}}g^{(5)}_{cc_1a,\boldsymbol{k}}\left(\omega\right)\right]$$

with

$$g^{(4)}_{acc_1,\boldsymbol{k}}\left(\omega\right)=\frac{e^3\bar{\omega}}{6}\left[\frac{1}{\left(\hbar\bar{\omega}-\Delta E_{ac,\boldsymbol{k}}\right)\left(2\hbar\bar{\omega}-\Delta E_{ac_1,\boldsymbol{k}}\right)}+\frac{1}{\left(\hbar\bar{\omega}+\Delta E_{ac,\boldsymbol{k}}\right)\left(2\hbar\bar{\omega}+\Delta E_{ac_1,\boldsymbol{k}}\right)}\right] \tag{30}$$

and

$$\begin{aligned}g^{(5)}_{cc_1a,\boldsymbol{k}}\left(\omega\right)=&\frac{e^3\bar{\omega}}{6}\left[\frac{1}{\left(\hbar\bar{\omega}-\Delta E_{cc_1,\boldsymbol{k}}\right)\left(2\hbar\bar{\omega}-\Delta E_{ca,\boldsymbol{k}}\right)}+\frac{1}{\left(\hbar\bar{\omega}+\Delta E_{cc_1,\boldsymbol{k}}\right)\left(2\hbar\bar{\omega}+\Delta E_{ca,\boldsymbol{k}}\right)}\right.\\&\left.+\frac{1}{\left(\hbar\bar{\omega}-\Delta E_{cc_1,\boldsymbol{k}}\right)\left(\hbar\bar{\omega}+\Delta E_{ca,\boldsymbol{k}}\right)}+\frac{1}{\left(\hbar\bar{\omega}+\Delta E_{cc_1,\boldsymbol{k}}\right)\left(\hbar\bar{\omega}-\Delta E_{ca,\boldsymbol{k}}\right)}\right].\end{aligned} \tag{31}$$

Here the superscript i in $A^{i}_{ac,\boldsymbol{k}}$ denotes the spatial component, the subscript l also denotes the spatial component, and $\hat{\partial}_{\boldsymbol{k}}$ is the generalized derivative operator [3]: $\hat{\partial}_{\boldsymbol{k}}\hat{S}_{ab,\boldsymbol{k}}=\left(\partial_{\boldsymbol{k}}-i\Delta\boldsymbol{A}_{ab,\boldsymbol{k}}\right)\hat{S}_{ab,\boldsymbol{k}}$. It is clear that $\gamma^{(1)}_{il}\left(\omega\right)$ in Eq. 24 accouts for the Fermi surface contribution, so it vanishes in an insulator. However, the remaining 4 terms are integrations over the occupied states and they are generally nonzero at finite frequency, leading to the nonlinear Hall effect in insulators. In fact, at the frequency near resonance, the nonvanishing nonlinear Hall conductivity in insulators is consistent with the breakdown of Kleinman symmetry in nonlinear optics [5, 6, 23].

SUPPLEMENTARY NOTE 4: THE BREAKDOWN OF KLEINMAN SYMMETRY AND THE NONLINEAR HALL EFFECT

In nonlinear optics, the Kleinman symmetry states that when the driving frequency is far below resonance, the indices of the nonlinear susceptibilities can be arbitrarily permuted [5, 6, 23]. For the optical second harmonic generation $P_q(2\omega) = \epsilon_0 \chi_{qij}(2\omega;\omega,\omega)\,\mathcal{E}_i(\omega)\,\mathcal{E}_j(\omega)$, it means that in far off-resonance, the indices of $\chi_{qij}(2\omega;\omega,\omega)$ respect the overall permutation symmetry. However, it is known that the Kleinman symmetry is an approximated symmetry that holds when the frequency dependence of the nonlinear susceptibility is negligible [5, 6]. Near resonance, the susceptibilities exhibit strong frequency dispersive properties, so the index q is no longer interchangeable with the indices i and j. The anti-symmetric part when interchanging q with i and j corresponds to the nonlinear Hall effect. According to the definition $\boldsymbol{J}(t) = d\boldsymbol{P}(t)/dt$, the conductivity and the susceptibility of the second harmonic generation respect the intrinsic relation:

$$\sigma_{qij}(2\omega;\omega,\omega) = -i2\omega\epsilon_0\chi_{qij}(2\omega;\omega,\omega), \tag{32}$$

so $\sigma_{qij}(2\omega;\omega,\omega)$ follows exactly the same form as $\chi_{qij}(2\omega;\omega,\omega)$ and also has the finite Hall component as that of $\chi_{qij}(2\omega;\omega,\omega)$ near resonance.

In the contracted notation, the optical second harmonic generation has the form [5, 6]

$$\begin{pmatrix} P_x(2\omega) \\ P_y(2\omega) \\ P_z(2\omega) \end{pmatrix} = \epsilon_0 \begin{pmatrix} d_{11} & d_{12} & d_{13} & d_{14} & d_{15} & d_{16} \\ d_{21} & d_{22} & d_{23} & d_{24} & d_{25} & d_{26} \\ d_{31} & d_{32} & d_{33} & d_{34} & d_{35} & d_{36} \end{pmatrix} \begin{pmatrix} \mathcal{E}_x^2(\omega) \\ \mathcal{E}_y^2(\omega) \\ \mathcal{E}_z^2(\omega) \\ 2\mathcal{E}_y(\omega)\mathcal{E}_z(\omega) \\ 2\mathcal{E}_x(\omega)\mathcal{E}_z(\omega) \\ 2\mathcal{E}_x(\omega)\mathcal{E}_y(\omega) \end{pmatrix}, \tag{33}$$

with

$$d_{11} = \chi_{xxx} \quad d_{12} = \chi_{xyy} \quad d_{13} = \chi_{xzz} \quad d_{14} = \chi_{xyz} \quad d_{15} = \chi_{xxz} \quad d_{16} = \chi_{xxy} \quad d_{21} = \chi_{yxx} \quad d_{22} = \chi_{yyy} \quad d_{23} = \chi_{yzz} \tag{34}$$

$$d_{24} = \chi_{yyz} \quad d_{25} = \chi_{yxz} \quad d_{26} = \chi_{yxy} \quad d_{31} = \chi_{zxx} \quad d_{32} = \chi_{zyy} \quad d_{33} = \chi_{zzz} \quad d_{34} = \chi_{zyz} \quad d_{35} = \chi_{zxz} \quad d_{36} = \chi_{zxy}. \tag{35}$$

Here χ_{ijk} with $i,j,k = x,y,z$ stands for the second harmonic susceptibility $\chi_{ijk}(2\omega;\omega,\omega)$, and the contracted susceptibility d_{il} is also frequency dependent (the frequencies are not written out for simplicity in notations). Constructing the longitudinal and transverse components of $\chi_{qij}(2\omega;\omega,\omega)$ follows exactly Eq. 12 and Eq. 13:

$$\chi^{\parallel}_{qij}(2\omega;\omega,\omega) = \frac{1}{3}\left[\chi_{qij}(2\omega;\omega,\omega) + \chi_{iqj}(2\omega;\omega,\omega) + \chi_{jiq}(2\omega;\omega,\omega)\right], \tag{36}$$

$$\chi^{\perp}_{qij}(2\omega;\omega,\omega) = \frac{1}{3}\left[2\chi_{qij}(2\omega;\omega,\omega) - \chi_{iqj}(2\omega;\omega,\omega) - \chi_{jiq}(2\omega;\omega,\omega)\right], \tag{37}$$

so combing Eq. 33 - Eq. 37, we obtain the longitudinal and transverse components of the contracted second harmonic susceptibility matrix:

$$d^{\parallel}_{il} = \frac{1}{3}\begin{pmatrix} 3d_{11} & d_{12}+2d_{26} & d_{13}+2d_{35} & d_{14}+d_{25}+d_{36} & 2d_{15}+d_{31} & 2d_{16}+d_{21} \\ d_{21}+2d_{16} & 3d_{22} & d_{23}+2d_{34} & 2d_{24}+d_{32} & d_{25}+d_{14}+d_{36} & 2d_{26}+d_{12} \\ d_{31}+2d_{15} & d_{32}+2d_{24} & 3d_{33} & 2d_{34}+d_{23} & 2d_{35}+d_{13} & d_{36}+d_{25}+d_{14} \end{pmatrix}, \tag{38}$$

and

$$d^{\perp}_{il} = \frac{1}{3}\begin{pmatrix} 0 & 2(d_{12}-d_{26}) & 2(d_{13}-d_{35}) & 2d_{14}-d_{25}-d_{36} & d_{15}-d_{31} & d_{16}-d_{21} \\ 2(d_{21}-d_{16}) & 0 & 2(d_{23}-d_{24}) & d_{24}-d_{32} & 2d_{25}-d_{14}-d_{36} & d_{26}-d_{12} \\ 2(d_{31}-d_{15}) & 2(d_{32}-d_{24}) & 0 & d_{34}-d_{23} & d_{35}-d_{13} & 2d_{36}-d_{14}-d_{25} \end{pmatrix}. \tag{39}$$

It is clear to check that $d_{il} = d^{\parallel}_{il} + d^{\perp}_{il}$. It is known that materials belonging to the 20 piezoelectric point groups can exhibit the second harmonic generation [5, 6, 24], and the specific forms of the second harmonic susceptibility tensor are listed in Table 1. With the help of Eq. 38 and Eq. 39, we also get the forms of the longitudinal and transverse components of the second harmonic susceptibility tensor for the 20 piezoelectric point groups, which are lsited in Table 2 and Table 3. We find that finite Hall component (or the transverse component) of the second harmonic generation is allowed to exist in 16 point groups: C_n, C_{nv}, $D_{n'}$, D_{2d} and S_4, with $n = 1,2,3,4,6$ and $n' = 2,3,4,6$. For the media belonging to the 16 point groups, the symmetry dicated that its second harmonic generation susceptibility always invovles the Hall component, and whether the media is an insulator or a metal does not matter. Near resonance, as the Kleinman symmetry breaks down, the Hall component of the second harmonic generation becomes significantly nonzero, indicating that the nonlinear Hall effect generally exists in insulators that belongs to the 16 point groups.

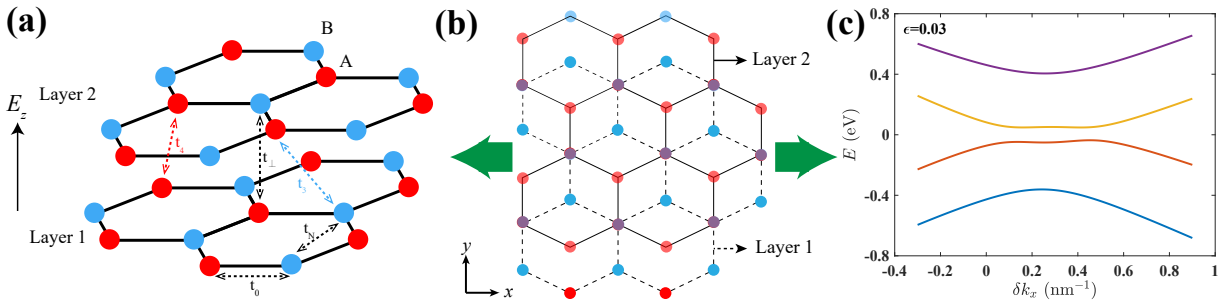

Supplementary Fig. 1: (a) The AB stacked (Bernal) bilayer graphene before adding the uniaxial strain. A z-directional electric field E_z is applied to induce a potential difference between the two layers. All the hoppings between the carbon atoms are labeled. (b) The top view of the Bernal bilayer graphene under uniaxial strain. The uniaxial strain is applied along the zigzag direction. The system respects the C_{1v} point group symmetry. (c) The band dispersions of the strained Bernal bilayer graphene. The uniaxial strain is set to be $\epsilon = 0.03$. The dispersions are plotted relative to the K valley: $\delta k_x = k_x - K_x$. In the energy spectrum, a gap of $\Delta = 84$ meV is introduced by the z-directional electric field.

SUPPLEMENTARY NOTE 5: THE NONLINEAR HALL EFFECT IN A GAPPED BERNAL BILAYER GRAPHENE

In the below, we choose the gapped Bernal bilayer graphene under uniaxial strain to demonstrate the nonlinear Hall effect in an insulator. The Bernal bilayer graphene originally belongs to the D_{3d} point group. Applying a z-directional electric field reduces the symmetry from D_{3d} to C_{3v}. The z-directional electric field can open a gap of $0 \sim 0.25$ eV in the energy spectrum of the Bernal bilayer graphene [25–28]. In a dual gate device, the chemical potential becomes gate tunable so that one can tune the chemical potential into the gap and make the Bernal bilayer graphene become insulating. Further applying a uniaxial strain breaks the C_3 symmetry, so the biased Bernal bilayer graphene becomes an insulator that falls into the 16 point groups that allow the nonvanishing nonlinear Hall effect. As shown in Fig. 1, the uniaxial strain in our model is applied along the zigzag direction (x-direction), so the Bernal bilayer system in our model respects the C_{1v} symmetry. The only remaining symmetry is the in-plane mirror that maps x to $-x$.

The Hamiltonian of the Biased Bernal Bilayer Grphane under Uniaxial Strain

The Bernal bilayer graphene is AB stacked as depicted in Fig. 1. In the basis of $(|\psi_{A_1,\boldsymbol{k}}\rangle, |\psi_{B_1,\boldsymbol{k}}\rangle, |\psi_{A_2,\boldsymbol{k}}\rangle, |\psi_{B_2,\boldsymbol{k}}\rangle)$, where the subscript $1,2$ denotes the layer index, one can write down the tight binding Hamiltonian of the Bernal bilayer graphene as [29, 30]

$$H(\boldsymbol{k}) = \begin{pmatrix} h_N(\boldsymbol{k}) + \Delta_0 & h_0(\boldsymbol{k}) & h_4(\boldsymbol{k}) & h_3(\boldsymbol{k}) \\ h_0^*(\boldsymbol{k}) & h_N(\boldsymbol{k}) + \Delta_0 + \Delta' & t_\perp & h_4(\boldsymbol{k}) \\ h_4^*(\boldsymbol{k}) & t_\perp & h_N(\boldsymbol{k}) - \Delta_0 + \Delta' & h_0(\boldsymbol{k}) \\ h_3^*(\boldsymbol{k}) & h_4^*(\boldsymbol{k}) & h_0^*(\boldsymbol{k}) & h_N(\boldsymbol{k}) - \Delta_0 \end{pmatrix}. \tag{40}$$

Here $t_\perp$ denotes the vertical hopping, Δ and Δ' are the layer dependent potential induced by the z-directional electric field. Other matrix elements in the Hamiltonian have the form

$$h_0(\boldsymbol{k}) = -t_{01}e^{i\boldsymbol{k}\cdot\boldsymbol{\delta}_1'} - t_{02}e^{-i\boldsymbol{k}\cdot\boldsymbol{\delta}_2'} - t_{03}e^{i\boldsymbol{k}\cdot\boldsymbol{\delta}_3'}, \tag{41}$$

$$h_N(\boldsymbol{k}) = -2t_{N1}\cos(\boldsymbol{k}\cdot\boldsymbol{a}_1') - 2t_{N_2}\cos(\boldsymbol{k}\cdot\boldsymbol{a}_2') - 2t_{N_3}\cos(\boldsymbol{k}\cdot\boldsymbol{a}_3'), \tag{42}$$

$$h_4(\boldsymbol{k}) = -t_{41}e^{i\boldsymbol{k}\cdot\boldsymbol{\delta}_1'} - t_{42}e^{i\boldsymbol{k}\cdot\boldsymbol{\delta}_2'} - t_{43}e^{i\boldsymbol{k}\cdot\boldsymbol{\delta}_3'}, \tag{43}$$

$$h_3(\boldsymbol{k}) = -t_{31}e^{-i\boldsymbol{k}\cdot\boldsymbol{\delta}_1'} - t_{32}e^{-i\boldsymbol{k}\cdot\boldsymbol{\delta}_2'} - t_{33}e^{-i\boldsymbol{k}\cdot\boldsymbol{\delta}_3'}. \tag{44}$$

The hopping parameters and the lattice site vectors are all modified by the uniaxial strain. Before adding strain, the lattice vectors connecting the nearest neighbor carbon atoms in the same layer are $\boldsymbol{\delta}_1 = (0,1)\,d$, $\boldsymbol{\delta}_2 = \left(-\frac{\sqrt{3}}{2}, -\frac{1}{2}\right)d$, $\boldsymbol{\delta}_3 = \left(\frac{\sqrt{3}}{2}, -\frac{1}{2}\right)d$, and those connecting the next nearest neighbor carbon atoms in the same layer are $\boldsymbol{a}_1 = \sqrt{3}\left(\frac{1}{2}, \frac{\sqrt{3}}{2}\right)d$, $\boldsymbol{a}_2 = \sqrt{3}\left(-\frac{1}{2}, \frac{\sqrt{3}}{2}\right)d$, $\boldsymbol{a}_3 = -\sqrt{3}\,(1,0)\,d$. Here $d = 1.42$Å denotes the distance between the neighboring carbon atoms.

For simplicity, we consider a homo-uniaxial tensile strain applied to the Bernal bilayer graphene. The strain tensor takes the form

$$\mathcal{E} = \epsilon \begin{pmatrix} \cos^2\theta' - \nu\sin^2\theta' & (1+\nu)\cos\theta'\sin\theta' \\ (1+\nu)\cos\theta'\sin\theta' & \sin^2\theta' - \nu\cos^2\theta' \end{pmatrix}, \tag{45}$$

with ϵ denoting the strain amplitude and $\nu = 0.165$ being the Poisson's ratio in graphite [31]. Here θ' is the angle between the strain applied direction and the zigzag direction (x-direction). As the uniaixal strain we considered is along the zigzag direction, the angle is set to be $\theta' = 0$ in the simulation. After applying the uniaxial strain, the three nearest neighbor bonding vectors become

$$\boldsymbol{\delta}_1' = \begin{pmatrix} 1+\mathcal{E}_{xx} & \mathcal{E}_{xy} \\ \mathcal{E}_{yx} & 1+\mathcal{E}_{yy} \end{pmatrix} \begin{pmatrix} 0 \\ 1 \end{pmatrix} d, \quad \boldsymbol{\delta}_2' = \begin{pmatrix} 1+\mathcal{E}_{xx} & \mathcal{E}_{xy} \\ \mathcal{E}_{yx} & 1+\mathcal{E}_{yy} \end{pmatrix} \begin{pmatrix} -\frac{\sqrt{3}}{2} \\ -\frac{1}{2} \end{pmatrix} d, \quad \boldsymbol{\delta}_3' = \begin{pmatrix} 1+\mathcal{E}_{xx} & \mathcal{E}_{xy} \\ \mathcal{E}_{yx} & 1+\mathcal{E}_{yy} \end{pmatrix} \begin{pmatrix} \frac{\sqrt{3}}{2} \\ -\frac{1}{2} \end{pmatrix} d, \tag{46}$$

and the three next nearest neighbor bonding vectors are changed to be

$$\boldsymbol{a}_1' = \begin{pmatrix} 1+\mathcal{E}_{xx} & \mathcal{E}_{xy} \\ \mathcal{E}_{xy} & 1+\mathcal{E}_{yy} \end{pmatrix} \begin{pmatrix} \frac{1}{2} \\ \frac{\sqrt{3}}{2} \end{pmatrix} \sqrt{3}d, \quad \boldsymbol{a}_2' = \begin{pmatrix} 1+\mathcal{E}_{xx} & \mathcal{E}_{xy} \\ \mathcal{E}_{xy} & 1+\mathcal{E}_{yy} \end{pmatrix} \begin{pmatrix} -\frac{1}{2} \\ \frac{\sqrt{3}}{2} \end{pmatrix} \sqrt{3}d, \quad \boldsymbol{a}_3' = \begin{pmatrix} 1+\mathcal{E}_{xx} & \mathcal{E}_{xy} \\ \mathcal{E}_{xy} & 1+\mathcal{E}_{yy} \end{pmatrix} \begin{pmatrix} -1 \\ 0 \end{pmatrix} \sqrt{3}d. \tag{47}$$

The hopping changes induced by the homo-uniaxial tensile strain are

$$t_{0i} = t_0 e^{-\beta_0\left[\frac{|\boldsymbol{\delta}_i'|}{d}-1\right]}, \quad t_{Ni} = t_N e^{-\beta_N\left[\frac{|\boldsymbol{a}_i'|}{\sqrt{3}d}-1\right]}, \quad t_{4i} = t_4 e^{-\beta_4\left[\frac{|\boldsymbol{\delta}_i'|}{d}-1\right]}, \quad t_{3i} = t_3 e^{-\beta_3\left[\frac{|\boldsymbol{\delta}_i'|}{d}-1\right]}, \tag{48}$$

where t_0, t_N, t_4 and t_3 are the hopping parameters before adding strain. Here $\beta_0 = 2$ and $\beta_N = \beta_4 = \beta_3 = 1$ are the Grüneisen parameters [30, 32, 33]. All the tight binding parameters before adding strain are set to take the values $t_0 = 3.16$ eV, $t_N = 0.3$ eV, $t_\perp = 0.38$ eV, $t_4 = 0.14$ eV, $t_3 = 0.38$ eV, $\Delta = 0.05$ eV, $\Delta' = 0.022$ eV [26, 27, 29, 30, 34, 35]. With the given parameters, one can plot the band dispersions of the biased Bernal bilayer graphene under the uniaxial strain $\epsilon = -0.03$, which is shown in Fig. 1 (c).

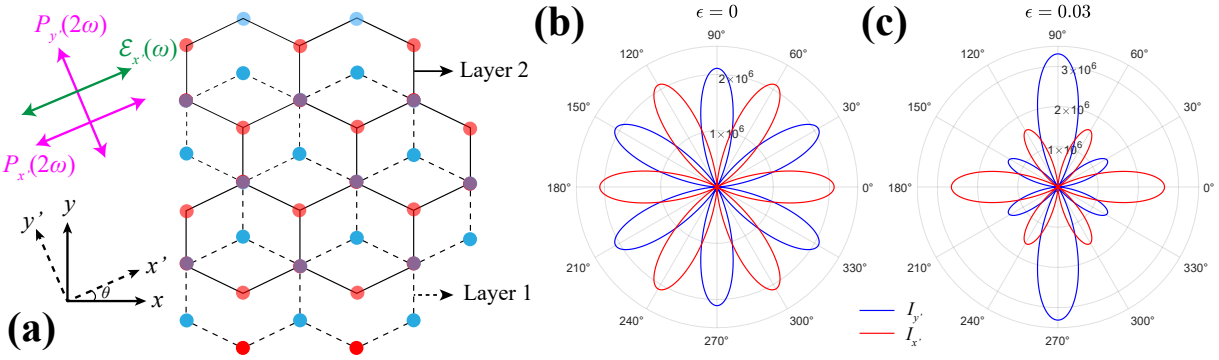

Supplementary Fig. 2: (a) The x' direction polarized input electric field and the resulting second harmonic generation $\boldsymbol{P}(2\omega) = [P_{x'}(2\omega), P_{y'}(2\omega)]$. The angle between the x' direction and the x direction (zigzag direction) is θ. In the second harmonic microscopy, one can fix the input electric field polarized in the x' direction and rotate the electric field polarization in the Bernal bilayer graphene plane to measure the second harmonic generation intensities in the parallel x' direction and the perpendicular y' direction respectively. In this way one can obtain the intensity of the secomd harmonics as a function of the polarization angle. (b) The polarplot of the second harmonic intensity from a biased Bernal bilayer graphene with no strain. (c) The polarplot of the second harmonic intensity from a biased Bernal bilayer graphene under a uniaxial strain applied along the zigzag direction. The second harmonic intensity is determined by the polarization of the second harmonics: $I_{x'} \propto P_{x'}^2$, $I_{y'} \propto P_{y'}^2$. Here the driving frequency is set to be $\hbar\omega = 40$ meV in the simulation.

Symmetry Analysis for the Second Harmonic Generation in Bernal Bilayer Graphene

For the Bernal bilayer graphene under a uniaxial strain applied along the zigzag direction (x-direction), Table 1 tells that an electric field polarized in the $x-y$ plane gives a second harmonic generation of the form

$$\begin{pmatrix} P_x(2\omega) \\ P_y(2\omega) \end{pmatrix} = \epsilon_0 \begin{pmatrix} 0 & 0 & -\chi(\omega) + \delta_1(\omega) + \delta_2(\omega) \\ -\chi(\omega) + \delta_1(\omega) - 2\delta_2(\omega) & \chi(\omega) & 0 \end{pmatrix} \begin{pmatrix} \mathcal{E}_x^2(\omega) \\ \mathcal{E}_y^2(\omega) \\ 2\mathcal{E}_x(\omega)\mathcal{E}_y(\omega) \end{pmatrix}. \tag{49}$$

Here $\chi(\omega)$ denotes the second harmonic generation before adding strain, while $\delta_1(\omega)$ and $\delta_2(\omega)$ correspond to the second harmonic generation arising from the C_3 symmetry breaking induced by the uniaxial strain. It is clear to see that $\chi_{xxy}(2\omega;\omega,\omega) = -\chi(\omega) + \delta_1(\omega) + \delta_2(\omega)$ and $\chi_{yxx}(2\omega;\omega,\omega) = -\chi(\omega) + \delta_1(\omega) - 2\delta_2(\omega)$, so $\chi_{xxy}(2\omega;\omega,\omega) \neq \chi_{yxx}(2\omega;\omega,\omega)$ as long as $\delta_2(\omega) \neq 0$. As a result, the key to detect the nonlinear Hall effect in this system is to measure the difference between $\chi_{xxy}(2\omega;\omega,\omega)$ and $\chi_{yxx}(2\omega;\omega,\omega)$.

The first step is to identify the crystalline axis. In a polarization resolved second harmonic microscopy setup [36–38], the polarization direction can rotate in the graphene plane (see Fig. 2), so one can measure the intensity of the second harmonic generation as a function of the polarization angle to identify the crystalline axis of the material. Let us set x' and y' to be the direction parallel and perpendicular to the polarizatioin direction respectively. Then the intensity of the second harmonic generation measured along the x' and y' direction becomes

$$I_{x'} \propto P_{x'}^2(2\omega) = \epsilon_0^2 E_{x'}^4(\omega)\left[-\chi(\omega)\sin 3\theta + 3\delta_1(\omega)\cos^2\theta\sin\theta\right]^2, \tag{50}$$

$$I_{y'} \propto P_{y'}^2(2\omega) = \epsilon_0^2 E_{y'}^4(\omega)\left[-\chi(\omega)\cos 3\theta + \frac{1}{4}\delta_1(\omega)(\cos\theta + 3\cos\theta) - 2\delta_2(\omega)\cos\theta\right]^2, \tag{51}$$

where θ denotes the angle between x' and the zigzag direction (x-direction). Before adding strain ($\epsilon = 0$), as the polarization direction rotates in the graphene plane, both $P_{x'}^2(2\omega)$ and $P_{y'}^2(2\omega)$ exhibit the C_3 symmetry as shown in Fig. 2 (b). After the uniaxial strain along the zigzag direction (x-direction) is applied, the C_3 symmetry in the polar plot of $I_{x'} \propto P_{x'}^2$ and $I_{y'} \propto P_{y'}^2$ disappears. As can be seen in Fig. 2 (c), when the polarization direction is parallel to the zigzag direction, $I_{x'}$ is maximal while $I_{y'}$ is the minimum. When the polarization direction is perpendicular to the zigzag direction, $I_{x'}$ gets the minimum value but $I_{y'}$ is the maximum. Such feature of the second harmonic generations in the polarplot identifies the zigzag direction of the strained Bernal bilayer graphene.

As the zigzag direction of the strained Bernal bilayer graphene of the C_{1v} symmetry can be identified by the polarization resolved second harmonic microscopy, one can proceed to detect the signature of the nonlinear Hall effect. One can first apply an electric field polarized in the x-direction: $\boldsymbol{\mathcal{E}}(\omega) = (1,0)\mathcal{E}(\omega)$ and then measure the second harmonic generation in the y direction

$$P_y(2\omega) = \epsilon_0\chi_{yxx}(2\omega;\omega,\omega)\mathcal{E}_x^2(\omega) = \epsilon_0\left[-\chi(\omega) + \delta_1(\omega) - 2\delta_2(\omega)\right]\mathcal{E}^2(\omega). \tag{52}$$

Then one can apply the electric field that polarized in the angular bisector line of the x and y direction: $\boldsymbol{\mathcal{E}}(\omega) = \frac{1}{\sqrt{2}}(1,1)\mathcal{E}(\omega)$ to measure the second harmonic generation in the x-direction:

$$P_x(2\omega) = \epsilon_0\chi_{xxy}(2\omega;\omega,\omega)2\mathcal{E}_x(\omega)\mathcal{E}_y(\omega) = \epsilon_0\left[-\chi(\omega) + \delta_1(\omega) + \delta_2(\omega)\right]\mathcal{E}^2(\omega). \tag{53}$$

It is evident that a nonzero $\delta_2(\omega)$ gives different values for the second harmonic intensities $I_x \propto P_x^2(2\omega)$ and $I_y \propto P_y^2(2\omega)$ measured in this way. The deviation between I_x and I_y identifies the anti-symmetric nature of the nonlinear Hall effect.

The Explicit Expressions for the Nonlinear Conductivities in the Biased Bernal Bilayer Graphene

In a two dimensional material, the Hall component of the second harmonic generation is given by

$$P_q^{\perp}(2\omega) = \left[\epsilon_{ljq}\tilde{\gamma}_{il}(\omega) + (i \leftrightarrow j)\right]\mathcal{E}_i(\omega)\mathcal{E}_j(\omega) \tag{54}$$

with $\tilde{\gamma}_{il}(\omega) = \frac{i}{2\omega\epsilon_0}\gamma_{il}(\omega)$. As the electric polarization is constrained in the $x-y$ plane, we can write the Hall component of the second harmonic generation in Eq. 54 explicitly out

$$\begin{pmatrix} P_x^{\perp}(2\omega) \\ P_y^{\perp}(2\omega) \end{pmatrix} = \begin{pmatrix} 0 & -2\tilde{\gamma}_{yz}(\omega) & -\tilde{\gamma}_{xz}(\omega) \\ 2\tilde{\gamma}_{xz}(\omega) & 0 & \tilde{\gamma}_{yz}(\omega) \end{pmatrix} \begin{pmatrix} \mathcal{E}_x^2(\omega) \\ \mathcal{E}_y^2(\omega) \\ 2\mathcal{E}_x(\omega)\mathcal{E}_y(\omega) \end{pmatrix}. \tag{55}$$

Comparing Eq. 55 with Eq. 49, we obtain

$$\chi_{xxy}^{\perp}(2\omega;\omega,\omega) = -\frac{1}{2}\chi_{yxx}^{\perp}(2\omega;\omega,\omega) = -\tilde{\gamma}_{xz}(2\omega;\omega,\omega) = \delta_2(\omega), \tag{56}$$

$$\chi_{xxy}^{\parallel}(2\omega;\omega,\omega) = \chi_{yxx}^{\parallel}(2\omega;\omega,\omega) = -\chi(\omega) + \delta_1(\omega), \tag{57}$$

$$\chi_{yyy}^{\parallel}(2\omega;\omega,\omega) = \chi_{yyy}(2\omega;\omega,\omega) = \chi(\omega). \tag{58}$$

Specifically, Eq, 56 clearly reveals the anti-symmetric nature of the Hall component of the second harmonic susceptibility.

For the strained Bernal bilayer graphene of the C_{1v} symmetry, the nonlinear Hall conductivity is determined by $\gamma_{xz}(2\omega;\omega,\omega)$. According to Eq. 23, we know that $\gamma_{xz}(2\omega;\omega,\omega)$ is composed of 5 terms:

$$\gamma_{xz}(\omega)=\gamma_{xz}^{(1)}(\omega)+\gamma_{xz}^{(2)}(\omega)+\gamma_{xz}^{(3)}(\omega)+\gamma_{xz}^{(4)}(\omega)+\gamma_{xz}^{(5)}(\omega), \tag{59}$$

and the explicit expression of each term takes the form

$$\gamma_{xz}^{(1)}(\omega)=\int_{\boldsymbol{k}}\sum_{a}\partial_{k_x}f_{a,\boldsymbol{k}}\sum_{c\neq a}\left(i\boldsymbol{A}_{ac,\boldsymbol{k}}\times\boldsymbol{A}_{ca,\boldsymbol{k}}\right)_z g_{ac,\boldsymbol{k}}^{(1)}(\omega), \tag{60}$$

$$\gamma_{xz}^{(2)}(\omega)=\int_{\boldsymbol{k}}\sum_{a,c\neq a}f_{a,\boldsymbol{k}}i\left[A_{ac,\boldsymbol{k}}^{x}\left(\hat{\partial}_{\boldsymbol{k}}\times\boldsymbol{A}_{ca,\boldsymbol{k}}\right)_z-\left(\hat{\partial}_{\boldsymbol{k}}\times\boldsymbol{A}_{ac,\boldsymbol{k}}\right)_z A_{ca,\boldsymbol{k}}^{x}+\partial_{k_x}\left(\boldsymbol{A}_{ac,\boldsymbol{k}}\times\boldsymbol{A}_{ca,\boldsymbol{k}}\right)_z\right]g_{ac,\boldsymbol{k}}^{(2)}(\omega), \tag{61}$$

$$\gamma_{xz}^{(3)}(\omega)=\int_{\boldsymbol{k}}\sum_{a,c\neq a}f_{a,\boldsymbol{k}}\left[i\left(\boldsymbol{A}_{ac,\boldsymbol{k}}\times\boldsymbol{A}_{ca,\boldsymbol{k}}\right)_z\Delta E_{ac,\boldsymbol{k}}\partial_{k_x}\Delta E_{ac,\boldsymbol{k}}\right]g_{ac,\boldsymbol{k}}^{(3)}(\omega), \tag{62}$$

$$\gamma_{xz}^{(4)}(\omega)=\int_{\boldsymbol{k}}\sum_{a,c\neq a,c_1\neq c,c_1\neq a}\left[A_{cc_1,\boldsymbol{k}}^{x}\left(i\boldsymbol{A}_{ac,\boldsymbol{k}}\times\boldsymbol{A}_{c_1a,\boldsymbol{k}}\right)_z-A_{c_1c,\boldsymbol{k}}^{x}\left(i\boldsymbol{A}_{ac_1,\boldsymbol{k}}\times\boldsymbol{A}_{ca,\boldsymbol{k}}\right)_z\right]\left[f_{a,\boldsymbol{k}}g_{acc_1,\boldsymbol{k}}^{(4)}(\omega)-f_{c,\boldsymbol{k}}g_{cc_1a,\boldsymbol{k}}^{(5)}(\omega)\right]. \tag{63}$$

The nonlinear Hall conductivity is then given by $\sigma_{xxy}^{\perp}(2\omega;\omega,\omega)=-\frac{1}{2}\sigma_{yxx}^{\perp}(2\omega;\omega,\omega)=-\gamma_{xz}(2\omega;\omega,\omega)$.

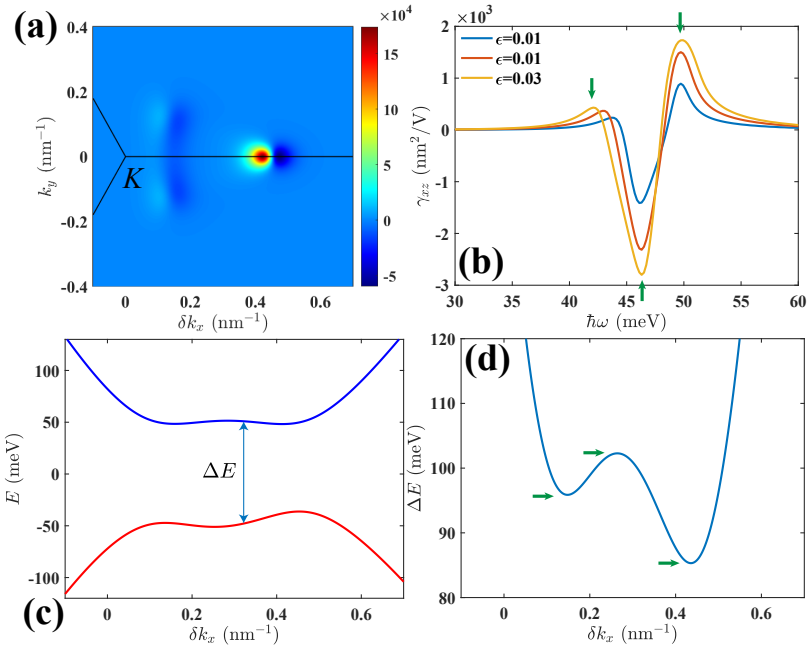

Supplementary Fig. 3: (a) The $\boldsymbol{k}$ space distribution of $\gamma_{xz}(\omega,\boldsymbol{k})$. The unit of $\gamma_{xz}(\omega,\boldsymbol{k})$ is mA·nm^3/V^2. The driving frequency is set to be $\hbar\omega=40$ meV and the strain amplitude is $\epsilon=0.03$. The nonzero $\gamma_{xz}(\boldsymbol{k},\omega)$ is found to mainly concentrate around the K. The black line denotes the Brillouin zone boundary. (b) $\gamma_{xz}(\omega)$ as a function of $\hbar\omega$. As strain amplitude increases, $\gamma_{xz}(\omega)$ that determines the nonlinear Hall conductivity also increases. Given $\epsilon=0.01$, the nonlinear Hall conductivity can reach 200 nm^2/V in the slightly off-resonant regime. The green arrows indicate the 3 local optimal values of $\gamma_{xz}(\omega)$. (c) The Mexican hat like bands of the biased Bernal bilayer graphene under uniaxial strain. The band dispersions are near the K valley with $\delta k_x=k_x-K_x$. (d) The energy difference between the empty conduction band and the occupied valence band. The green arrows label the 3 local optimal values of $\Delta E(\boldsymbol{k})$.

For the longitudinal component of the second harmonic conductivity, there are three terms: $\sigma_{xxy}^{\parallel}(2\omega;\omega,\omega)$, $\sigma_{yxx}^{\parallel}(2\omega;\omega,\omega)$ and $\sigma_{yyy}^{\parallel}(2\omega;\omega,\omega)$. The first two terms are equivalent: $\sigma_{xxy}^{\parallel}(2\omega;\omega,\omega)=\sigma_{yxx}^{\parallel}(2\omega;\omega,\omega)$, so one only needs to calculate two terms: $\sigma_{xxy}^{\parallel}(2\omega;\omega,\omega)$ and $\sigma_{yyy}^{\parallel}(2\omega;\omega,\omega)$. Combing Eq. 7 and Eq. 12, we have

$$\sigma_{xxy}^{\parallel}(2\omega;\omega,\omega)=\sigma_{xxy}^{\parallel,(1)}(2\omega;\omega,\omega)+\sigma_{xxy}^{\parallel,(2)}(2\omega;\omega,\omega)+\sigma_{xxy}^{\parallel,(3)}(2\omega;\omega,\omega), \tag{64}$$

with

$$\sigma^{\parallel,(1)}_{xxy}\left(2\omega;\omega,\omega\right)=-\frac{e^3}{2\hbar^3}\frac{\tau^2}{\left(1-i\omega\tau\right)^2}\int_{\boldsymbol{k}}f_{a,\boldsymbol{k}}\partial_{k_x}\partial_{k_x}\partial_{k_y}E_{a,\boldsymbol{k}}, \tag{65}$$

$$\begin{aligned}\sigma^{\parallel,(2)}_{xxy}\left(2\omega;\omega,\omega\right)=&\frac{1}{3}\int_{\boldsymbol{k}}\sum_{a,c\neq a}f_{a,\boldsymbol{k}}\Big(A^{y}_{ac,\boldsymbol{k}}\hat{\partial}_{k_x}A^{x}_{ca,\boldsymbol{k}}-\hat{\partial}_{k_x}A^{x}_{ac,\boldsymbol{k}}\cdot A^{y}_{ca,\boldsymbol{k}}+A^{x}_{ac,\boldsymbol{k}}\hat{\partial}_{k_x}A^{y}_{ca,\boldsymbol{k}}-\hat{\partial}_{k_x}A^{y}_{ac,\boldsymbol{k}}\cdot A^{x}_{ca,\boldsymbol{k}}\\&+A^{x}_{ac,\boldsymbol{k}}\hat{\partial}_{k_y}A^{x}_{ca,\boldsymbol{k}}-\hat{\partial}_{k_y}A^{x}_{ac,\boldsymbol{k}}\cdot A^{x}_{ca,\boldsymbol{k}}\Big)g^{\parallel,(2)}_{ac,\boldsymbol{k}}\left(\omega\right),\end{aligned} \tag{66}$$

$$\begin{aligned}\sigma^{\parallel,(3)}_{xxy}\left(2\omega;\omega,\omega\right)=&\frac{i}{3}\int_{\boldsymbol{k}}\sum_{a}f_{a,\boldsymbol{k}}\Big(A^{y}_{ac,\boldsymbol{k}}A^{x}_{cc_1,\boldsymbol{k}}A^{x}_{c_1a,\boldsymbol{k}}+A^{x}_{ac_1,\boldsymbol{k}}A^{x}_{c_1c,\boldsymbol{k}}A^{y}_{ca,\boldsymbol{k}}+A^{x}_{ac,\boldsymbol{k}}A^{y}_{cc_1,\boldsymbol{k}}A^{x}_{c_1a,\boldsymbol{k}}+A^{x}_{ac_1,\boldsymbol{k}}A^{y}_{c_1c,\boldsymbol{k}}A^{x}_{ca,\boldsymbol{k}}\\&+A^{x}_{ac,\boldsymbol{k}}A^{x}_{cc_1,\boldsymbol{k}}A^{y}_{c_1a}+A^{y}_{ac_1,\boldsymbol{k}}A^{x}_{c_1c,\boldsymbol{k}}A^{x}_{ca,\boldsymbol{k}}\Big)g^{\parallel,(3)}_{acc_1,\boldsymbol{k}}\left(\omega\right),\end{aligned} \tag{67}$$

and

$$\sigma^{\parallel}_{yyy}\left(2\omega;\omega,\omega\right)=\sigma^{\parallel,(1)}_{yyy}\left(2\omega;\omega,\omega\right)+\sigma^{\parallel,(2)}_{yyy}\left(2\omega;\omega,\omega\right)+\sigma^{\parallel,(3)}_{yyy}\left(2\omega;\omega,\omega\right), \tag{68}$$

with

$$\sigma^{\parallel,(1)}_{yyy}\left(2\omega;\omega,\omega\right)=-\frac{e^3}{2\hbar^3}\frac{\tau^2}{\left(1-i\omega\tau\right)^2}\int_{\boldsymbol{k}}f_{a,\boldsymbol{k}}\partial_{k_y}\partial_{k_y}\partial_{k_y}E_{a,\boldsymbol{k}}, \tag{69}$$

$$\sigma^{\parallel,(2)}_{yyy}\left(2\omega;\omega,\omega\right)=\int_{\boldsymbol{k}}\sum_{a}f_{a,\boldsymbol{k}}\left(A^{y}_{ac,\boldsymbol{k}}\hat{\partial}_{k_y}A^{y}_{ca,\boldsymbol{k}}-\hat{\partial}_{k_y}A^{y}_{ac,\boldsymbol{k}}\cdot A^{y}_{ca,\boldsymbol{k}}\right)g^{\parallel,(2)}_{ac,\boldsymbol{k}}\left(\omega\right), \tag{70}$$

$$\sigma^{\parallel,(3)}_{yyy}\left(2\omega;\omega,\omega\right)=\int_{\boldsymbol{k}}\sum_{a}f_{a,\boldsymbol{k}}\left(A^{y}_{ac,\boldsymbol{k}}A^{y}_{cc_1,\boldsymbol{k}}A^{y}_{c_1a,\boldsymbol{k}}+A^{y}_{ac_1,\boldsymbol{k}}A^{y}_{c_1c,\boldsymbol{k}}A^{y}_{ca,\boldsymbol{k}}\right)g^{\parallel,(3)}_{acc_1,\boldsymbol{k}}\left(\omega\right). \tag{71}$$

Here the frequency dependent form factors are

$$g^{\parallel,(2)}_{ac,\boldsymbol{k}}\left(\omega\right)=\frac{e^3\bar{\omega}}{\hbar^2\bar{\omega}^2-\left(\Delta E_{ac,\boldsymbol{k}}\right)^2}-\frac{e^3\bar{\omega}}{\left(\hbar\bar{\omega}-\Delta E_{ac,\boldsymbol{k}}\right)\left(2\hbar\bar{\omega}-\Delta E_{ac,\boldsymbol{k}}\right)}-\frac{e^3\bar{\omega}}{\left(\hbar\bar{\omega}+\Delta E_{ac,\boldsymbol{k}}\right)\left(2\hbar\bar{\omega}+\Delta E_{ac,\boldsymbol{k}}\right)}, \tag{72}$$

and

$$\begin{aligned}g^{\parallel,(3)}_{acc_1,\boldsymbol{k}}\left(\omega\right)=&\frac{e^3\bar{\omega}}{\left(\hbar\bar{\omega}-\Delta E_{ac,\boldsymbol{k}}\right)\left(2\hbar\bar{\omega}-\Delta E_{ac_1,\boldsymbol{k}}\right)}+\frac{e^3\bar{\omega}}{\left(\hbar\bar{\omega}+\Delta E_{ac,\boldsymbol{k}}\right)\left(2\hbar\bar{\omega}+\Delta E_{ac_1,\boldsymbol{k}}\right)}\\&-\frac{e^3\bar{\omega}}{\left(\hbar\bar{\omega}-\Delta E_{ac,\boldsymbol{k}}\right)\left(2\hbar\bar{\omega}-\Delta E_{c_1c,\boldsymbol{k}}\right)}-\frac{e^3\bar{\omega}}{\left(\hbar\bar{\omega}+\Delta E_{ac,\boldsymbol{k}}\right)\left(2\hbar\bar{\omega}+\Delta E_{c_1c,\boldsymbol{k}}\right)}.\end{aligned} \tag{73}$$

As Eq. 59-Eq. 71 involve both the transverse (Hall) and longitudinal components, the conductivity of the second harmonic generation can then be obtained: $\sigma_{xxy}\left(2\omega;\omega,\omega\right)=\sigma^{\perp}_{xxy}\left(2\omega;\omega,\omega\right)+\sigma^{\parallel}_{xxy}\left(2\omega;\omega,\omega\right)$, $\sigma_{yxx}\left(2\omega;\omega,\omega\right)=\sigma^{\perp}_{yxx}\left(2\omega;\omega,\omega\right)+\sigma^{\parallel}_{yxx}\left(2\omega;\omega,\omega\right)$, and $\sigma_{yyy}\left(2\omega;\omega,\omega\right)=\sigma^{\parallel}_{yyy}\left(2\omega;\omega,\omega\right)$. With Eq. 32, we can obtain $\chi_{xxy}\left(2\omega;\omega,\omega\right)$, $\chi_{yxx}\left(2\omega;\omega,\omega\right)$ and $\chi_{yyy}\left(2\omega;\omega,\omega\right)$ accordingly. In our calculation, since we focus on the insulating state with no Fermi surface, we take the relaxation free limit $\tau^{-1}\to 0^{+}$ to perform the calculation.

In Fig. 3 (a), we plot $\gamma_{xz}\left(\omega,\boldsymbol{k}\right)$, which shows the $\boldsymbol{k}$ space distribution for the integrand of $\gamma_{xz}\left(\omega\right)$ in Eq. 59. It is clear to see that nonzero $\gamma_{xz}\left(\omega\right)$ mainly concentrate around the K (and $-K$) valley. In Fig. 3 (b), we plot $\gamma_{xz}\left(\omega\right)$ as a function of the driving frequency. As the uniaxial strain amplitude increases, the C_3 symmetry gets more broken so that $\gamma_{xz}\left(\omega\right)$ increases. It is noteworthy that $\gamma_{xz}\left(\omega\right)$ can reach 200 nm^2/V given a small strain amplitude $\epsilon=0.01$. From Fig. 3 (b), one can find that $\gamma_{xz}\left(\omega\right)$ has 3 local optimal values. Those 3 local optimal values stem from the Mexican hat shape of the bands as seen in Fig. 3 (c). The energy difference between the empty conduction band and the occupied valence band is plotted in Fig. 3 (d), which shows 3 local optimal values in $\Delta E\left(\boldsymbol{k}\right)$ as well. Each time when the frequency $2\hbar\omega$ approaches to one local optimal value of $\Delta E\left(\boldsymbol{k}\right)$ labeled by the arrows in Fig. 3 (d), the corresponding second harmonic generation gets accordingly optimized. Therefore, as the driving frequency increases from zero, the resulting second harmonic susceptibility $\gamma_{xz}\left(\omega\right)$ increases to reach the first local maxima, then decrease to reach the local minima, and finally reach the second local maxima, as depicted in Fig. 3 (b) and Fig. 2 (c). A supplementary video is attached to show how $\gamma_{xz}\left(\omega,\boldsymbol{k}\right)$ evolves with the driving frequency.

[1] D. J. Passos, G. B. Ventura, J. M. Viana Parente Lopes, J. M. B. Lopes dos Santos, and N. M. R. Peres, Phys. Rev. B **97**, 235446 (2018).
[2] J. E. Sipe and E. Ghahramani, Phys. Rev. B **48**, 11705 (1993).
[3] C. Aversa and J. E. Sipe, Phys. Rev. B **52**, 14646 (1995).
[4] G. B. Ventura, D. J. Passos, J. M. B. Lopes dos Santos, J. M. Viana Parente Lopes, and N. M. R. Peres, Phys. Rev. B **96**, 035431 (2017).
[5] R. Boyd, *Nonlinear Optics* (Academic Press, 2020).
[6] P. N. Butcher and D. Cotter, *The Elements of Nonlinear Optics* (Cambridge University Press, 2003).
[7] E. L. Ivchenko and G. Pikus, *Superlattices and Other Heterostructures, Symmetry and Optical Phenomena* (Springer Verlag, Berlin, Heildelberg, 1995).
[8] Q. Ma et al., Nature **565**, 337 (2019).
[9] K. Kang, T. Li, E. Sohn, J. Shan, and K. F. Mak, Nat. Mater. **18**, 324 (2019).
[10] P. He, S. S.-L. Zhang, D. Zhu, S. Shi, O. G. Heinonen, G. Vignale, and H. Yang, Phys. Rev. Lett. **123**, 016801 (2019).
[11] D. Kumar, C.-H. Hsu, R. Sharma, T.-R. Chang, P. Yu, J. Wang, G. Eda, G. Liang, and H. Yang, Nat. Nanotech. **16** (2021).
[12] S.-C. Ho, C.-H. Chang, Y.-C. Hsieh, S.-T. Lo, B. Huang, T.-H.-Y. Vu, C. Ortix, and T.-M. Chen, Nat. Electron. **4**, 116 (2021).
[13] J. Duan, Y. Jian, Y. Gao, H. Peng, J. Zhong, Q. Feng, J. Mao, and Y. Yao, Phys. Rev. Lett. **129**, 186801 (2022).
[14] M. Huang et al., Natl. Sci. Rev. nwac232 (2022).
[15] M. Huang, Z. Wu, X. Zhang, X. Feng, Z. Zhou, S. Wang, Y. Chen, C. Chen, K. Sun, Z. Y. Meng, and N. Wang, Phys. Rev. Lett. **131**, 066301 (2023).
[16] L. Min, H. Tan, Z. Xie, L. Miao, R. Zhang, S. H. Lee, V. Gopalan, C.-X. Liu, N. Alem, B. Yan, and Z. Mao, Nat. Commun. **14**, 364 (2023).
[17] S. Sinha et al., Nat. Phys. **18**, 765 (2022).
[18] X.-G. Ye, H. Liu, P.-F. Zhu, W.-Z. Xu, S. A. Yang, N. Shang, K. Liu, and Z.-M. Liao, Phys. Rev. Lett. **130**, 016301 (2023).
[19] B. Chen, Y. Gao, Z. Zheng, S. Chen, Z. Liu, L. Zhang, Q. Zhu, H. Li, L. Li, and C. Zeng, Nat. Commun. **15**, 5513 (2024).
[20] X. F. Liu, C.-P. Zhang, N. Wang, D. Zhao, X. Zhou, W. Gao, X. H. Chen, K. T. Law, and K. P. Loh, Nat. Commun. **15**, 245 (2024).
[21] A. Gao, Y.-F. Liu, J.-X. Qiu, B. Ghosh, T. V. Trevisan, Y. Onishi, C. Hu, T. Qian, H.-J. Tien, and S.-W. Chen et al., Science **381**, 181 (2023).
[22] N. Wang, D. Kaplan, Z. Zhang, T. Holder, N. Cao, A. Wang, X. Zhou, F. Zhou, Z. Jiang, and C. Zhang et al., Nature **621**, 487 (2023).
[23] D. A. Kleinman, Phys. Rev. B **128**, 1761 (1962).
[24] R. Newnham, *Properties of materials: anisotropy, symmetry and structure* (Oxford University Press Inc., New York, 2005).
[25] K. F. Mak, C. H. Lui, J. Shan, and T. F. Heinz, Phys. Rev. Lett. **102**, 256405 (2009).
[26] E. V. Castro, K. S. Novoselov, S. V. Morozov, N. M. R. Peres, J. M. B. Lopes dos Santos, J. Nilsson, F. Guinea, A. K. Geim, and A. H. Castro Neto, Phys. Rev. Lett. **99**, 216802 (2007).
[27] Y. Zhang, T.-T. Tang, C. Girit, Z. Hao, M. C. Martin, A. Zettl, M. F. Crommie, Y. R. Shen, and F. Wang, Nature **459**, 820 (2009).
[28] J. Velasco et al., Nat. Nanotechnol. **7**, 156 (2012).
[29] E. McCann and M. Koshino, Rep. Prog. Phys. **76**, 056503 (2013).
[30] B. T. Schaefer and K. C. Nowack, Phys. Rev. B **103**, 224426 (2021).
[31] V. M. Pereira, A. H. Castro Neto, and N. M. R. Peres, Phys. Rev. B **80**, 045401 (2009).
[32] G. G. Naumis, S. Barraza-Lopez, M. Oliva-Leyva, and H. Terrones, Rep. Prog. Phys. **80**, 096501 (2017).
[33] R. Battilomo, N. Scopigno, and C. Ortix, Phys. Rev. Lett. **123**, 196403 (2019).
[34] A. B. Kuzmenko, I. Crassee, D. Marel, P. Blake, and K. S. Novoselov, Phys. Rev. B **80**, 165406 (2009).
[35] A. H. Castro Neto, F. Guinea, N. M. R. Peres, K. S. Novoselov, and A. K. Geim, Rev. Mod. Phys. **81**, 109 (2009).
[36] N. Kumar, S. Najmaei, Q. Cui, F. Ceballos, P. M. Ajayan, J. Lou, and H. Zhao, Phys. Rev. B **87**, 161403 (R) (2013).
[37] L. M. Malard, T. V. Alencar, A. P. M. Barboza, K. F. Mak, and A. M. de Paula, Phys. Rev. B **87**, 201401 (R) (2013).
[38] Y. Li, Y. Rao, K. F. Mak, Y. You, S. Wang, C. R. Dean, and T. F. Heinz, Nano Lett. **13**, 3329 (2013).

Supplementary Table 1: The 20 piezoelectric point groups that allow the second harmonic generation. The corresponding forms of the second harmonic generation susceptibilities are presented in the contracted notation.

Point group	Contracted matrix d_{il}	Coordinate notation
C_1	$\begin{pmatrix} d_{11} & d_{12} & d_{13} & d_{14} & d_{15} & d_{16} \\ d_{21} & d_{22} & d_{23} & d_{24} & d_{25} & d_{26} \\ d_{31} & d_{32} & d_{33} & d_{34} & d_{35} & d_{36} \end{pmatrix}$	arbitrary
C_2	$\begin{pmatrix} 0 & 0 & 0 & d_{14} & 0 & d_{16} \\ d_{21} & d_{22} & d_{23} & 0 & d_{25} & 0 \\ 0 & 0 & 0 & d_{34} & 0 & d_{36} \end{pmatrix}$	2-fold rotation along y
$C_{1h} = C_s = C_{1v}$	$\begin{pmatrix} 0 & 0 & 0 & 0 & d_{15} & d_{16} \\ d_{21} & d_{22} & d_{23} & d_{24} & 0 & 0 \\ d_{31} & d_{32} & d_{33} & d_{34} & 0 & 0 \end{pmatrix}$	in-plane mirror $x \to -x$
C_{2v}	$\begin{pmatrix} 0 & 0 & 0 & 0 & d_{15} & 0 \\ 0 & 0 & 0 & d_{24} & 0 & 0 \\ d_{31} & d_{32} & d_{33} & 0 & 0 & 0 \end{pmatrix}$	2-fold rotation along z, in-plane mirror $x \to -x$, $y \to -y$
$D_2 = V$	$\begin{pmatrix} 0 & 0 & 0 & d_{14} & 0 & 0 \\ 0 & 0 & 0 & 0 & d_{25} & 0 \\ 0 & 0 & 0 & 0 & 0 & d_{36} \end{pmatrix}$	three 2-fold rotation axes along x, y, z
C_3	$\begin{pmatrix} d_{11} & -d_{11} & 0 & d_{14} & d_{15} & -d_{22} \\ -d_{22} & d_{22} & 0 & d_{15} & -d_{14} & -d_{11} \\ d_{31} & d_{31} & d_{33} & 0 & 0 & 0 \end{pmatrix}$	3-fold rotation axis along z
D_3	$\begin{pmatrix} d_{11} & -d_{11} & 0 & d_{14} & 0 & 0 \\ 0 & 0 & 0 & 0 & -d_{14} & -d_{11} \\ 0 & 0 & 0 & 0 & 0 & 0 \end{pmatrix}$	3-fold rotation axis along z, 2-fold rotation axis along x
C_{3v}	$\begin{pmatrix} 0 & 0 & 0 & 0 & d_{15} & -d_{22} \\ -d_{22} & d_{22} & 0 & d_{15} & 0 & 0 \\ d_{31} & d_{31} & d_{33} & 0 & 0 & 0 \end{pmatrix}$	3-fold rotation along z, in-plane mirror: $x \to -x$
C_4, C_6	$\begin{pmatrix} 0 & 0 & 0 & d_{14} & d_{15} & 0 \\ 0 & 0 & 0 & d_{15} & -d_{14} & 0 \\ d_{31} & d_{31} & d_{33} & 0 & 0 & 0 \end{pmatrix}$	rotation axis along z
S_4	$\begin{pmatrix} 0 & 0 & 0 & d_{14} & -d_{15} & 0 \\ 0 & 0 & 0 & d_{15} & d_{14} & 0 \\ d_{31} & -d_{31} & 0 & 0 & 0 & d_{36} \end{pmatrix}$	improper rotation axis along z
C_{4v}, C_{6v}	$\begin{pmatrix} 0 & 0 & 0 & 0 & d_{15} & 0 \\ 0 & 0 & 0 & d_{15} & 0 & 0 \\ d_{31} & d_{31} & d_{33} & 0 & 0 & 0 \end{pmatrix}$	rotation axis along z, in-plane mirror: $x \to -x$
D_4, D_6	$\begin{pmatrix} 0 & 0 & 0 & d_{14} & 0 & 0 \\ 0 & 0 & 0 & 0 & -d_{14} & 0 \\ 0 & 0 & 0 & 0 & 0 & 0 \end{pmatrix}$	4-fold,6-fold rotation axis along z, 2-fold rotation axis along x
$D_{2d} = V_d$	$\begin{pmatrix} 0 & 0 & 0 & d_{14} & 0 & 0 \\ 0 & 0 & 0 & 0 & d_{14} & 0 \\ 0 & 0 & 0 & 0 & 0 & d_{36} \end{pmatrix}$	three 2-fold rotation axes along x, y, z, in-plane mirror $x \to y, y \to x$
$C_{3h} = S_3$	$\begin{pmatrix} d_{11} & -d_{11} & 0 & 0 & 0 & -d_{22} \\ -d_{22} & d_{22} & 0 & 0 & 0 & -d_{11} \\ 0 & 0 & 0 & 0 & 0 & 0 \end{pmatrix}$	3-fold rotation axis along z
D_{3h}	$\begin{pmatrix} 0 & 0 & 0 & 0 & 0 & -d_{22} \\ -d_{22} & d_{22} & 0 & 0 & 0 & 0 \\ 0 & 0 & 0 & 0 & 0 & 0 \end{pmatrix}$	3-fold rotation axis along z, 2-fold rotation axis along y
T_d, T	$\begin{pmatrix} 0 & 0 & 0 & d_{14} & 0 & 0 \\ 0 & 0 & 0 & 0 & d_{14} & 0 \\ 0 & 0 & 0 & 0 & 0 & d_{14} \end{pmatrix}$	(x, y, z) along crystal axis (a, b, c)

Supplementary Table 2: The longitudinal components of the second harmonic generation susceptibilities in Supplementary Table 1. The contracted matrix forms of the longitudinal second harmonic generation susceptibilities are constructed from Eq. 38. The coordinate choice is the same as Supplementary Table 1.

Point group	Contracted matrix $d_{\parallel,il}$
C_1	$\frac{1}{3}\begin{pmatrix} 3d_{11} & d_{12}+2d_{26} & d_{13}+2d_{35} & d_{14}+d_{25}+d_{36} & 2d_{15}+d_{31} & 2d_{16}+d_{21} \\ d_{21}+2d_{16} & 3d_{22} & d_{23}+2d_{34} & 2d_{24}+d_{32} & d_{25}+d_{14}+d_{36} & 2d_{26}+d_{12} \\ d_{31}+2d_{15} & d_{32}+2d_{24} & 3d_{33} & 2d_{34}+d_{23} & 2d_{35}+d_{13} & d_{36}+d_{25}+d_{14} \end{pmatrix}$
C_2	$\frac{1}{3}\begin{pmatrix} 0 & 0 & 0 & d_{14}+d_{25}+d_{36} & 0 & 2d_{16}+d_{21} \\ d_{21}+2d_{16} & 3d_{22} & d_{23}+2d_{34} & 0 & d_{25}+d_{14}+d_{36} & 0 \\ 0 & 0 & 0 & 2d_{34}+d_{23} & 0 & d_{36}+d_{14}+d_{35} \end{pmatrix}$
$C_{1h}=C_s=C_{1v}$	$\frac{1}{3}\begin{pmatrix} 0 & 0 & 0 & 0 & 2d_{15}+d_{31} & 2d_{16}+d_{21} \\ 2d_{16}+d_{21} & d_{22} & d_{23}+2d_{34} & 2d_{24}+d_{32} & 0 & 0 \\ 2d_{15}+d_{31} & 2d_{24}+d_{32} & 3d_{33} & d_{23}+2d_{34} & 0 & 0 \end{pmatrix}$
C_{2v}	$\frac{1}{3}\begin{pmatrix} 0 & 0 & 0 & 0 & 2d_{15}+d_{31} & 0 \\ 0 & 0 & 0 & 2d_{24}+d_{32} & 0 & 0 \\ d_{31}+2d_{15} & d_{32}+2d_{24} & 3d_{33} & 0 & 0 & 0 \end{pmatrix}$
$D_2=V$	$\frac{1}{3}\begin{pmatrix} 0 & 0 & 0 & d_{14}+d_{25}+d_{36} & 0 & 0 \\ 0 & 0 & 0 & 0 & d_{25}+d_{14}+d_{36} & 0 \\ 0 & 0 & 0 & 0 & 0 & d_{36}+d_{14}+d_{25} \end{pmatrix}$
C_3	$\frac{1}{3}\begin{pmatrix} 3d_{11} & -3d_{11} & 0 & 0 & 2d_{15}+d_{31} & -3d_{22} \\ -3d_{22} & 3d_{22} & 0 & 2d_{15}+d_{31} & 0 & -3d_{11} \\ d_{31}+2d_{15} & d_{31}+2d_{15} & 3d_{33} & 0 & 0 & 0 \end{pmatrix}$
D_3	$\begin{pmatrix} d_{11} & -d_{11} & 0 & 0 & 0 & 0 \\ 0 & 0 & 0 & 0 & 0 & -d_{11} \\ 0 & 0 & 0 & 0 & 0 & 0 \end{pmatrix}$
C_{3v}	$\frac{1}{3}\begin{pmatrix} 0 & 0 & 0 & 0 & 2d_{15}+d_{31} & -3d_{22} \\ -3d_{22} & 3d_{22} & 0 & 2d_{15}+d_{31} & 0 & 0 \\ d_{31}+2d_{15} & d_{31}+2d_{15} & 3d_{33} & 0 & 0 & 0 \end{pmatrix}$
C_4, C_6	$\frac{1}{3}\begin{pmatrix} 0 & 0 & 0 & 0 & 2d_{15}+d_{31} & 0 \\ 0 & 0 & 0 & 2d_{15}+d_{31} & 0 & 0 \\ 2d_{15}+d_{31} & 2d_{15}+d_{31} & 3d_{33} & 0 & 0 & 0 \end{pmatrix}$
S_4	$\frac{1}{3}\begin{pmatrix} 0 & 0 & 0 & 2d_{14}+d_{36} & -2d_{15}+d_{31} & 0 \\ 0 & 0 & 0 & 2d_{15}-d_{31} & 2d_{14}+d_{36} & 0 \\ d_{31}-2d_{15} & -d_{31}+2d_{15} & 0 & 0 & 0 & d_{36}+2d_{14} \end{pmatrix}$
C_{4v}, C_{6v}	$\frac{1}{3}\begin{pmatrix} 0 & 0 & 0 & 0 & 2d_{15}+d_{31} & 0 \\ 0 & 0 & 0 & 2d_{15}+d_{31} & 0 & 0 \\ d_{31}+2d_{15} & d_{31}+2d_{15} & 3d_{33} & 0 & 0 & 0 \end{pmatrix}$
D_4, D_6	$\begin{pmatrix} 0 & 0 & 0 & 0 & 0 & 0 \\ 0 & 0 & 0 & 0 & 0 & 0 \\ 0 & 0 & 0 & 0 & 0 & 0 \end{pmatrix}$
$D_{2d}=V_d$	$\frac{1}{3}\begin{pmatrix} 0 & 0 & 0 & 2d_{14}+d_{36} & 0 & 0 \\ 0 & 0 & 0 & 0 & 2d_{14}+d_{36} & 0 \\ 0 & 0 & 0 & 0 & 0 & d_{36}+2d_{14} \end{pmatrix}$
$C_{3h}=S_3$	$\begin{pmatrix} d_{11} & -d_{11} & 0 & 0 & 0 & -d_{22} \\ -d_{22} & d_{22} & 0 & 0 & 0 & -d_{11} \\ 0 & 0 & 0 & 0 & 0 & 0 \end{pmatrix}$
D_{3h}	$\begin{pmatrix} 0 & 0 & 0 & 0 & 0 & -d_{22} \\ -d_{22} & d_{22} & 0 & 0 & 0 & 0 \\ 0 & 0 & 0 & 0 & 0 & 0 \end{pmatrix}$
T_d, T	$\begin{pmatrix} 0 & 0 & 0 & d_{14} & 0 & 0 \\ 0 & 0 & 0 & 0 & d_{14} & 0 \\ 0 & 0 & 0 & 0 & 0 & d_{14} \end{pmatrix}$

Supplementary Table 3: The transverse components of the second harmonic susceptibilities in Supplementary Table 1. The contracted matrix forms of the longitudinal second harmonic generation susceptibilities are constructed from Eq. 39. The coordinate choice is the same as Supplementary Table 1.

Point group	Contracted matrix $d_{\perp,il}$
C_1	$\frac{1}{3}\begin{pmatrix} 0 & 2(d_{12}-d_{26}) & 2(d_{13}-d_{35}) & 2d_{14}-d_{25}-d_{36} & d_{15}-d_{31} & d_{16}-d_{21} \\ 2(d_{21}-d_{16}) & 0 & 2(d_{23}-d_{34}) & d_{24}-d_{32} & 2d_{25}-d_{14}-d_{36} & d_{26}-d_{12} \\ 2(d_{31}-d_{15}) & 2(d_{32}-d_{24}) & 0 & d_{34}-d_{23} & d_{35}-d_{13} & 2d_{36}-d_{14}-d_{25} \end{pmatrix}$
C_2	$\frac{1}{3}\begin{pmatrix} 0 & 0 & 0 & 2d_{14}-d_{25}-d_{36} & 0 & d_{16}-d_{21} \\ 2(d_{21}-d_{16}) & 0 & 2(d_{23}-d_{34}) & 0 & 2d_{25}-d_{14}-d_{36} & 0 \\ 0 & 0 & 0 & d_{34}-d_{23} & 0 & 2d_{36}-d_{14}-d_{25} \end{pmatrix}$
$C_{1h} = C_s = C_{1v}$	$\frac{1}{3}\begin{pmatrix} 0 & 0 & 0 & 0 & d_{15}-d_{31} & d_{16}-d_{21} \\ 2(d_{21}-d_{16}) & 0 & 2(d_{23}-d_{34}) & d_{24}-d_{32} & 0 & 0 \\ 2(d_{31}-d_{15}) & 2(d_{32}-d_{24}) & 0 & d_{34}-d_{23} & 0 & 0 \end{pmatrix}$
C_{2v}	$\frac{1}{3}\begin{pmatrix} 0 & 0 & 0 & 0 & d_{15}-d_{31} & 0 \\ 0 & 0 & 0 & d_{24}-d_{32} & 0 & 0 \\ 2(d_{31}-d_{15}) & 2(d_{32}-d_{24}) & 0 & 0 & 0 & 0 \end{pmatrix}$
$D_2 = V$	$\frac{1}{3}\begin{pmatrix} 0 & 0 & 0 & 2d_{14}-d_{25}-d_{36} & 0 & 0 \\ 0 & 0 & 0 & 0 & 2d_{25}-d_{14}-d_{36} & 0 \\ 0 & 0 & 0 & 0 & 0 & 2d_{36}-d_{14}-d_{25} \end{pmatrix}$
C_3	$\frac{1}{3}\begin{pmatrix} 0 & 0 & 0 & 3d_{14} & d_{15}-d_{31} & 0 \\ 0 & 0 & 0 & d_{15}-d_{31} & -3d_{14} & 0 \\ 2(d_{31}-d_{15}) & 2(d_{31}-d_{15}) & 0 & 0 & 0 & 0 \end{pmatrix}$
D_3	$\begin{pmatrix} 0 & 0 & 0 & d_{14} & 0 & 0 \\ 0 & 0 & 0 & 0 & -d_{14} & 0 \\ 0 & 0 & 0 & 0 & 0 & 0 \end{pmatrix}$
C_{3v}	$\frac{1}{3}\begin{pmatrix} 0 & 0 & 0 & 0 & d_{15}-d_{31} & 0 \\ 0 & 0 & 0 & d_{15}-d_{31} & 0 & 0 \\ 2(d_{31}-d_{15}) & 2(d_{31}-d_{15}) & 0 & 0 & 0 & 0 \end{pmatrix}$
C_4, C_6	$\frac{1}{3}\begin{pmatrix} 0 & 0 & 0 & 3d_{14} & d_{15}-d_{31} & 0 \\ 0 & 0 & 0 & d_{15}-d_{31} & -3d_{14} & 0 \\ 2(d_{31}-d_{15}) & 2(d_{31}-d_{15}) & d_{33} & 0 & 0 & 0 \end{pmatrix}$
S_4	$\frac{1}{3}\begin{pmatrix} 0 & 0 & 0 & d_{14}-d_{36} & -d_{15}-d_{31} & 0 \\ 0 & 0 & 0 & d_{15}+d_{31} & d_{14}-d_{36} & 0 \\ 2(d_{31}+d_{15}) & -2(d_{31}+d_{15}) & 0 & 0 & 0 & 2(d_{36}-d_{14}) \end{pmatrix}$
C_{4v}, C_{6v}	$\frac{1}{3}\begin{pmatrix} 0 & 0 & 0 & 0 & d_{15}-d_{31} & 0 \\ 0 & 0 & 0 & d_{15}-d_{31} & 0 & 0 \\ 2(d_{31}-d_{15}) & 2(d_{31}-d_{15}) & 0 & 0 & 0 & 0 \end{pmatrix}$
D_4, D_6	$\begin{pmatrix} 0 & 0 & 0 & d_{14} & 0 & 0 \\ 0 & 0 & 0 & 0 & -d_{14} & 0 \\ 0 & 0 & 0 & 0 & 0 & 0 \end{pmatrix}$
$D_{2d} = V_d$	$\frac{1}{3}\begin{pmatrix} 0 & 0 & 0 & d_{14}-d_{36} & 0 & 0 \\ 0 & 0 & 0 & 0 & d_{14}-d_{36} & 0 \\ 0 & 0 & 0 & 0 & 0 & 2(d_{36}-d_{14}) \end{pmatrix}$
$C_{3h} = S_3$	$\begin{pmatrix} 0 & 0 & 0 & 0 & 0 & 0 \\ 0 & 0 & 0 & 0 & 0 & 0 \\ 0 & 0 & 0 & 0 & 0 & 0 \end{pmatrix}$
D_{3h}	$\begin{pmatrix} 0 & 0 & 0 & 0 & 0 & 0 \\ 0 & 0 & 0 & 0 & 0 & 0 \\ 0 & 0 & 0 & 0 & 0 & 0 \end{pmatrix}$
T_d, T	$\begin{pmatrix} 0 & 0 & 0 & 0 & 0 & 0 \\ 0 & 0 & 0 & 0 & 0 & 0 \\ 0 & 0 & 0 & 0 & 0 & 0 \end{pmatrix}$